ACS OMEGA

http://pubs.acs.org/journal/acsodf

Article

Distinguishing Asphyxia from Sudden Cardiac Death as the Cause of Death from the Lung Tissues of Rats and Humans Using Fourier Transform Infrared Spectroscopy

Kai Zhang, Ruina Liu, Ya Tuo, Kaijun Ma, Dongchuan Zhang, Zhenyuan Wang,* and Ping Huang*

Cite This: *ACS Omega* 2022, 7, 46859−46869

Read Online

ACCESS | Metrics & More | Article Recommendations | Supporting Information

ABSTRACT: The ability to determine asphyxia as a cause of death is important in forensic practice and helps us to judge whether a case is criminal. However, in some cases where the deceased has underlying heart disease, death by asphyxia cannot be determined by traditional autopsy and morphological observation under a microscope because there are no specific morphological features for either asphyxia or sudden cardiac death (SCD). Here, Fourier transform infrared (FTIR) spectroscopy was employed to distinguish asphyxia from SCD. A total of 40 lung tissues (collected at 0 h and 24 h postmortem) from 20 rats (10 died from asphyxia and 10 died from SCD) and 16 human lung tissues from 16 real cases were used for spectral data acquisition. After data preprocessing, 2675 spectra from rat lung tissues and 1526 spectra from human lung tissues were obtained for subsequent analysis. First, we found that there were biochemical differences in the rat lung tissues between the two causes of death by principal component analysis and partial least-squares discriminant analysis (PLS-DA), which were related to alterations in lipids, proteins, and nucleic acids. In addition, a PLS-DA classification model can be built to distinguish asphyxia from SCD. Second, based on the spectral data obtained from lung tissues allowed to decompose for 24 h, we could still distinguish asphyxia from SCD even when decomposition occurred in animal models. Nine important spectral features that contributed to the discrimination in the animal experiment were selected and further analyzed. Third, 7 of the 9 differential spectral features were also found to be significantly different in human lung tissues from 16 real cases. A support vector machine model was finally built by using the seven variables to distinguish asphyxia from SCD in the human samples. Compared with the linear PLS-DA model, its accuracy was significantly improved to 0.798, and the correct rate of determining the cause of death was 100%. This study shows the application potential of FTIR spectroscopy for exploring the subtle biochemical differences resulting from different death processes and determining the cause of death even after decomposition.

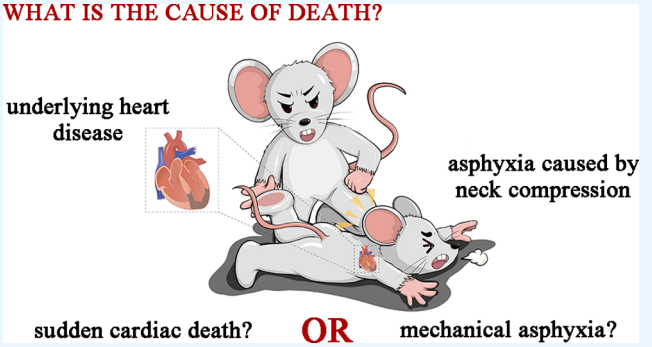

INTRODUCTION

Determining the cause of death is an important aspect of forensic practice. Asphyxia as a cause of death, however, is difficult to diagnose because the asphyxiation signs on the body can be non-specific or inapparent sometimes, especially in cases of manual strangulation, smothering, or positional asphyxia. The determination of asphyxia[1−3] as a cause of death is concluded by excluding other causes of death, according to histological and toxicological assessments and scene settings. However, the deceased may have underlying heart disease that can result in unexpected sudden cardiac death (SCD). Then, asphyxia will be harder to determine because there are also no specific or representative indicators for SCD. In reality, we often face problems in distinguishing between asphyxia and SCD, as asphyxia is a common violent cause of death, occurring and causing high death rates, and SCD is a global public health issue, resulting in many deaths.[4−7]

At present, most studies on the determination of asphyxia use molecular biological techniques to find differentially expressed mRNAs, miRNAs, or proteins, such as dual-specificity phosphatase 1 (*DUSP1*)/potassium voltage-gated channel subfamily J member 2 (*KCNJ2*),[8] miRNA-122,[9] miRNA-3185,[10,11] surfactant protein A (SP-A),[12] hypoxia-inducible factor-1α (HIF-1α),[13] glucose transporter 1/vascular endothelial growth factor,[14] aquaporin-5,[15] cytochrome C/apoptosis inducing factor,[16] and migration inhibitory factor-related protein-8/-14 (MRP-8/-14).[17] The same is true for SCD.[18−21] However, these biomolecules cannot be applied in

Received: September 15, 2022
Accepted: November 23, 2022
Published: December 7, 2022

practical work yet because their sensitivity and specificity necessitate further investigation, as well as the potential effect of postmortem degradation on their content change and diagnostic ability is unknown and remains to be studied. Two recent studies by our research team investigated the potential of mass spectrometry (MS)-based metabolomics to distinguish asphyxia from SCD.[22,23] However, the sample pretreatment and data collection of MS-based metabolomics are time-consuming and expensive.

Fourier transform infrared (FTIR) spectroscopy is a rapid, inexpensive, non-destructive, and relatively simple technique that can be utilized to analyze biomolecules qualitatively and quantitatively in biological studies.[24] The spectra detected can be used to characterize the biochemical status of samples so that subtle biochemical differences can be explored. This technique is widely used in the biomedical field.[25−28] As an example, cancerous tissues and noncancerous tissues can be distinguished by FTIR spectroscopy for cancer diagnosis, which can help doctors diagnose tumors or guide surgical resection scopes during tumor resection surgery.[29−33]

Moreover, FTIR spectroscopy is widely used in forensic science,[34,35] especially in forensic pathology.[36−40] Studies have focused on the determination of complex causes of death. Lin et al. and Wu et al. detected pulmonary edema fluid by FTIR imaging and constructed classification models for determining SCD,[41] anaphylactic shock,[42] hypothermia,[43] or diabetic ketoacidosis[44] as the cause. Tuo et al.[45] and Wang et al.[46] studied the vitreous fluid and liver tissue, respectively, of animal models of fatal hyperthermia and proposed FTIR spectroscopy as an alternative for determining the cause of death. These reports proved the application potential of FTIR spectroscopy in determining complex causes of death and inspired us to distinguish asphyxia from SCD as the cause of death. However, none of these studies evaluate the effect of decomposition, preventing FTIR spectroscopy from being applied to determine the cause of death in practice. In most cases, corpses may exhibit varying degrees of autolysis and putrefaction because of different postmortem intervals (PMIs), environmental temperatures, healthy conditions, and so on.[47] Therefore, the effect of decomposition on the determination of causes of death by FTIR spectroscopy needs to be studied.

The lung is one of the most important organs in the respiratory system and is affected by asphyxia. We hypothesize that the lung biochemical changes caused by asphyxia are different from those caused by cardiac arrest and that this difference can be detected by FTIR spectroscopy. Therefore, in this study, FTIR spectroscopy was used to detect biochemical differences in fresh and decomposed lung tissues of rats who died of asphyxia or SCD, and chemometric methods were used to construct classification models to distinguish asphyxia as the cause of death. Moreover, spectra of human samples were obtained to validate the results of animal experiments and test the practical application potential of FTIR spectroscopy.

MATERIALS AND METHODS

Animal Experiment and Sample Preparation. Twenty male Sprague−Dawley rats (weighing 230−270 g) were commercially provided (randomly chosen) from the Animal Center of Xi'an Jiaotong University. The experimental animals were kept in a temperature-controlled (Ta, 25 ± 3 °C) environment with a 12 h light/dark cycle and were given food and water ad libitum before the modeling. Based on the cause of death, the rats were randomized into asphyxia and SCD groups (10 rats per group), as well as calibration and prediction sets (7 rats as the calibration set and 3 rats as the prediction set for both the asphyxia and SCD groups). An intraperitoneal injection of urethane (20%, 1.0−1.2 g/kg) was administered to guarantee sufficient anesthesia in each rat to make sure that they experienced minimal pain along with discomfort prior to being sacrificed. This work was approved by the Laboratory Animal Management Committee of Xi'an Jiaotong University.

In the asphyxia group, ligature strangulation was used to construct the model. We placed a noose derived from cotton thread around the neck of each rat, and we inserted a small stick into the noose at the back of the neck. After that, tightening of the noose was done via rotation of the stick to asphyxiate each rat in the presence of constant pressure until the rat died (between 3.8 and 5.3 min, mean value: 4.4 min, standard deviation: 0.4 min). In the SCD group, coronary ligation was used to cause acute myocardial ischemia. Each rat's thorax and pericardium were cut to reveal the heart first. Then, the left anterior descending coronary artery was ligatured, causing the rat to die between 6.7 and 10.2 min (mean value: 8.5 min, standard deviation: 1.0 min). Hemostatic operations were performed during the time.

For each rat, part of the lung tissue was collected after confirming death and then stored at −80 °C. Then, the wound was sewn up, and the cadaver was placed inside an incubator (temperature, 25 ± 3 °C; humidity, 50% ± 5%) for 24 h (we selected one time-point to study preliminarily the effect of decomposition). The rest of the lung tissue, which had decomposed, was then obtained and stored at −80 °C until use. Before the FTIR imaging measurement, the fresh and decomposed lung tissues were taken from the freezer, and 10 μm thick sections of the lung were cut with a cryo-microtome at −20 °C and were thawed on an infrared transparent calcium fluoride (CaF_2) slide and then air-dried for approximately 5 min.

Moreover, human lung tissues from 16 cases (death from asphyxia, n = 6; death from SCD, n = 10) were collected from real forensic pathologic autopsies at the Academy of Forensic Science, Shanghai Public Security Bureau, and Xi'an Jiaotong University. The cause of death in the cases was diagnosed by forensic pathologists through a systematic forensic autopsy examination, including macroscopic morphological, histological, and toxicological examinations, taking into account the death process and medical history. The PMI of these cadavers ranged from approximately 12 h to 3 days, as shown in Table S1. Human lung tissue samples were made into frozen sections with the aforementioned method.

FTIR Imaging Acquisition. The spectroscopic chemical imaging data were acquired in transmission mode with the Hyperion 3000 FTIR Spectrometer (Bruker Optics, Ettlingen, Germany), which is equipped with a liquid nitrogen-cooled mercury−cadmium−telluride focal plane array detector with 4096 pixels in 64 × 64 grid format. Using a 15× objective with 0.4 NA, the spatial resolution of each pixel was 2.6 × 2.6 μm^2. The spectra were collected between 3950 and 900 cm^{-1} (spectral resolution of 4 cm^{-1}). Before the acquisition of each sample, the background was scanned 128 times from a clean blank area of the CaF_2 slides and was averaged. Then, the samples were scanned 64 times, and the averaged absorbance spectra were obtained (the background signal was automatically subtracted). For each tissue section, six tissue areas were captured and scanned with 4 × 4 binning (spectra that were

https://doi.org/10.1021/acsomega.2c05968
ACS Omega 2022, 7, 46859−46869

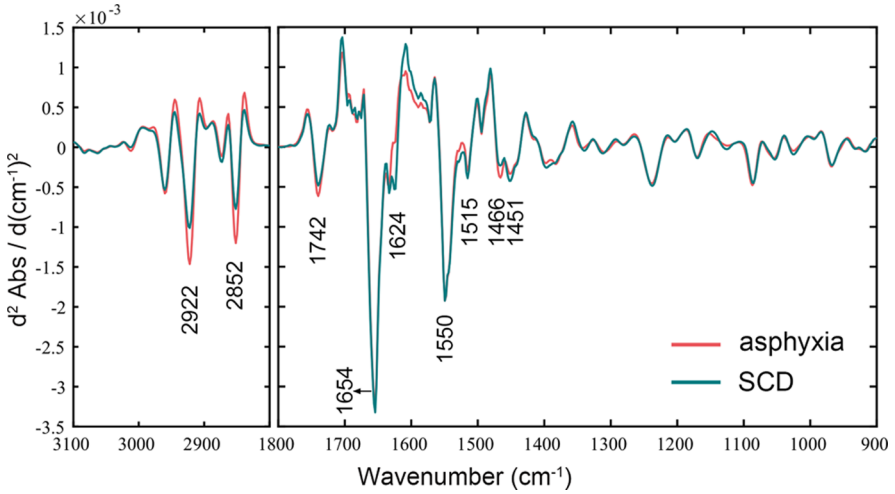

Figure 1. Comparison of the average second derivative spectra of lung tissues in rats who died from asphyxia (red) or SCD (green). SCD: sudden cardiac death.

collected corresponding to 4 × 4 pixels were combined into a single spectrum, therefore there are 256 spectra per area; each spectrum represented the sample information in the range of 10.4 × 10.4 μm^2), as shown in Figure S1 in the Online Resource 1. Consequently, a total of 240 infrared imaging data (61,440 spectra) were collected from 40 tissue sections of the lung samples (including fresh and decomposed samples) of 20 rats in the asphyxia and SCD groups. A total of 96 infrared imaging data (24,576 spectra) were collected from 16 tissue sections of human lung tissue samples from 16 real cases.

Data Preprocessing. By performing data preprocessing, the robustness and interpretability of subsequent data analysis can be enhanced.[48] First, a quality test was employed for every imaging data to remove the spectra with a low signal-to-noise ratio (SNR) or spectra with too low or too high absorbance intensity. The SNR threshold value was set to 200, which was calculated as the ratio of the maximum signal intensity in the amide I region (1700−1600 cm^{-1}) to the standard deviation in 1900−1800 cm^{-1}. The maximum absorbance intensity in the protein amide region (1700−1500 cm^{-1}) was checked, and the threshold value was set at 1.0 and 0.2 (the upper and lower thresholds, respectively). Second, the qualified spectra were converted to second-derivative spectra by use of the Savitzki−Golay (SG) algorithm[49] (11 points of smoothing) to address the issue of spectral overlap (the original average spectra are shown in Figure S2) and then normalized by the extended multiplicative signal correction (EMSC) algorithm to make the data more comparable.[50] Third, the data outside the wavenumber ranges of 3100−2800 and 1800−900 cm^{-1} were deleted to reduce the variable numbers. These two regions contain the spectral absorption bands of the main biomolecules of interest, such as lipids, proteins, carbohydrates, and nucleic acids.[51] Finally, every 20 spectra of the rat dataset were randomly selected and averaged to form a single spectrum, while it is every 15 spectra in the human dataset (the averaging operation is to reduce the measurement variance and the number of spectra to facilitate the subsequent data processing and analysis; the choice of the average parameter is arbitrary as long as the number of resulting spectra is suitable).

As a result, for animal samples, a preprocessed calibration set (containing 499, 419, 416, and 499 averaged spectra corresponding to the asphyxia, SCD, asphyxia-decomposed, and SCD-decomposed groups, respectively) and a preprocessed external validation/prediction set (containing 222, 202, 180, and 224 averaged spectra corresponding to the asphyxia, SCD, asphyxia-decomposed, and SCD-decomposed groups, respectively) were obtained and subjected to the following data analysis. For human samples, we obtained a preprocessed dataset containing 623 and 903 averaged spectra corresponding to asphyxia and SCD, respectively.

Data Analysis. As a classical unsupervised pattern recognition algorithm, principal component analysis (PCA) is usually performed as the first step to calculate principal components (PCs), which are the linear combinations of the original variables, to reduce the data dimensionality. The overall clustering, distinction, and variations of the dataset can also be visualized by projecting samples onto the two-dimensional or three-dimensional PC space.[52] In this study, PCA was employed to characterize the spectral profiles of the asphyxia and SCD groups after data scaling of the mean center. According to the resultant PC score plot, we can preliminarily explore if there is a difference between the lung tissues of rats from the two causes of death. In addition, the outliers (about 10%) were identified and removed from the dataset according to the leverage values and *Q*-residuals.[53]

Supervised linear partial least-squares discriminant analysis (PLS-DA)[54] was used to construct classification models to distinguish the two causes of death. The model was built by use of the spectra in the training set. A 10-fold cross-validation (CV) procedure was performed to select the number of latent variables (LVs) to obtain a better discrimination and prediction performance.[55] To evaluate the prediction performance, the spectra from the test set were subjected to the model. Moreover, according to the regression coefficients, the differential spectral variables that contributed to the distinction between the asphyxia and SCD groups can be explored.

Subsequently, the relative peak intensities of these bands were compared at different PMIs after overall normalization. The statistical significance of the differences was assessed by the Mann−Whitney *U* test (a nonparametric method) since the data failed to pass the normality test and the homogeneity test of variance. A *P* value <0.05 was considered significantly

https://doi.org/10.1021/acsomega.2c05968
ACS Omega 2022, 7, 46859−46869

different. In addition, the differences in these bands were also checked in human samples.

Last, we tried to classify the human sample data as originating from the asphyxia or SCD group by use of those differential spectral variables. The spectral data of 2 asphyxia cases and 3 SCD cases were randomly selected as the test dataset, and the rest (4 asphyxia cases and 7 SCD cases) were used as the modeling dataset. Although the number of real cases is not large, the number of spectra collected from these human samples is 1,526 (after preprocessing), which is enough to train a classification model. Linear PLS-DA models and nonlinear support vector machine discriminant analysis (SVM-DA) models were built here and evaluated by internal CV and external validation/prediction. The model accuracy was calculated based on the confusion matrix during the prediction process, whose formula is equal to (TP + TN)/(TP + TN + FP + FN) (TP: true positive; TN: true negative; FP: false positive; FN: false negative). The sensitivity is equal to TP/(TP + FN), and the specificity is equal to TN/(FP + TN). Receiver operating characteristics (ROC) curve analysis was utilized to calculate the areas under the curve (AUCs) in the PLS-DA and SVM-DA models. DeLong's test was performed to calculate the statistical significance of the improvement in AUC.[56]

Software. Data preprocessing and analysis were performed using MATLAB R2017b (MathWorks, MA, USA) equipped with the MIA Toolbox 1.0 (Eigenvector Research, WA, USA) and the DeLongUI[57] toolbox (https://github.com/PamixSun/DeLongUI). The statistical analysis was performed using IBM SPSS Statistics Version 20 (IBM corporation, NY, USA).

RESULTS

Characterization of the Spectral Differences between the Asphyxia and SCD Groups. The EMSC normalized and averaged second-derivative spectra for the lung tissues of the asphyxia and SCD groups were compared, as shown in Figure 1. Due to the preprocessing of the second-derivative, the direction of all peaks is reversed. The larger the absolute value of the peak is, the higher the relative content of biomolecules it represents. The peak shapes were similar at first glance, but obvious differences could be observed in the spectral region of lipids (3100−2800 cm^{-1}). There were also some slight differences around the bands at 1742, 1624, 1466, and 1451 cm^{-1}.

A PCA model was constructed to further reveal the overall variances between the two causes of death based on the second-derivative spectra. The PCA result is displayed in Figure 2. In the PCA score plots, each point in multidimensional space represents a single spectrum that contains rich biochemical information after dimensional reduction. As shown in Figure 2, although there is a slight overlap, the lung tissue spectra in the asphyxia group are clearly separated from those in the SCD group in the direction of PC-1, which accounts for 68.61% of the total variance.

A binary PLS-DA classification model was established to discriminate between the spectra of the asphyxia and SCD groups. The Venetian blind CV procedure was applied to the PLS-DA model to select the number of LVs. Three LVs were used to construct the PLS-DA model, as shown in Figure S3a. The prediction score and regression coefficient plots are shown in Figure 3. In the score plot, the model threshold, which decides whether a sample corresponds to the current class, is shown by the black dotted line. Almost all spectra of the asphyxia group lie above the cutoff line, entirely splitting from the spectra of the SCD group. Figure 3b shows the regression coefficient of the PLS-DA model. The wavenumbers with high absolute values of coefficients are important for classification,[54] so the regression coefficient plot displays the spectral variables contributing to the separation. The negatively correlated bands for the SCD group are mainly found at 1624 cm^{-1}, whereas the positively correlated bands for the asphyxia group are mainly found at 2922, 2852, 1742, 1706, and 1609 cm^{-1}. The result is basically consistent with the result in Figure 1. In addition, the external validation/test set was subjected to the PLS-DA model to assess the robustness and the true predictive capability spectra. A clear discrimination distribution is still observed around the threshold line.

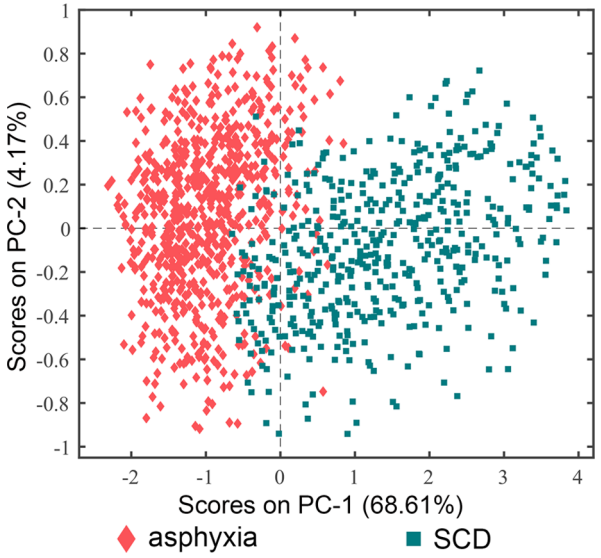

Figure 2. Result of PCA applied to spectra of lung tissues in rats who died from asphyxia (red) or SCD (green). PC-1 accounts for 68.61% of the total variance.

Classification Model and Effect of Decomposition. Another PLS-DA model was established to explore the discrimination when decomposition occurred by use of the spectra of the asphyxia-decomposed and SCD-decomposed groups (two LVs). The plot of the classification error rate versus the number of LVs is shown in Figure S3b. The plots of prediction score and regression coefficient are illustrated in Figure 4. The spectra of the two groups are completely separated. According to the coefficient plot, the negatively correlated loadings for the SCD group mainly show at 1713, 1649, 1624, and 1536 cm^{-1}, whereas the positively correlated loadings for the asphyxia group mainly show at 2922, 2852, 1742, 1706, and 1609 cm^{-1}. Additionally, the PLS-DA model of the decomposed samples (which is abbreviated as "the decomposed PLS-DA model" for writing convenience, and that of the fresh samples is the "fresh PLS-DA model") displays a good prediction ability in the external validation.

Moreover, some of the spectral variables that contribute to the discrimination are consistent with those in the fresh PLS-DA model, and some are more pronounced. Nine bands were selected and their relative peak intensities were further compared in fresh and decomposed lung samples, as shown in Figure 5.

Validation with Human Samples. The relative peak intensities of the nine bands in the human sample dataset were

https://doi.org/10.1021/acsomega.2c05968
ACS Omega 2022, 7, 46859−46869

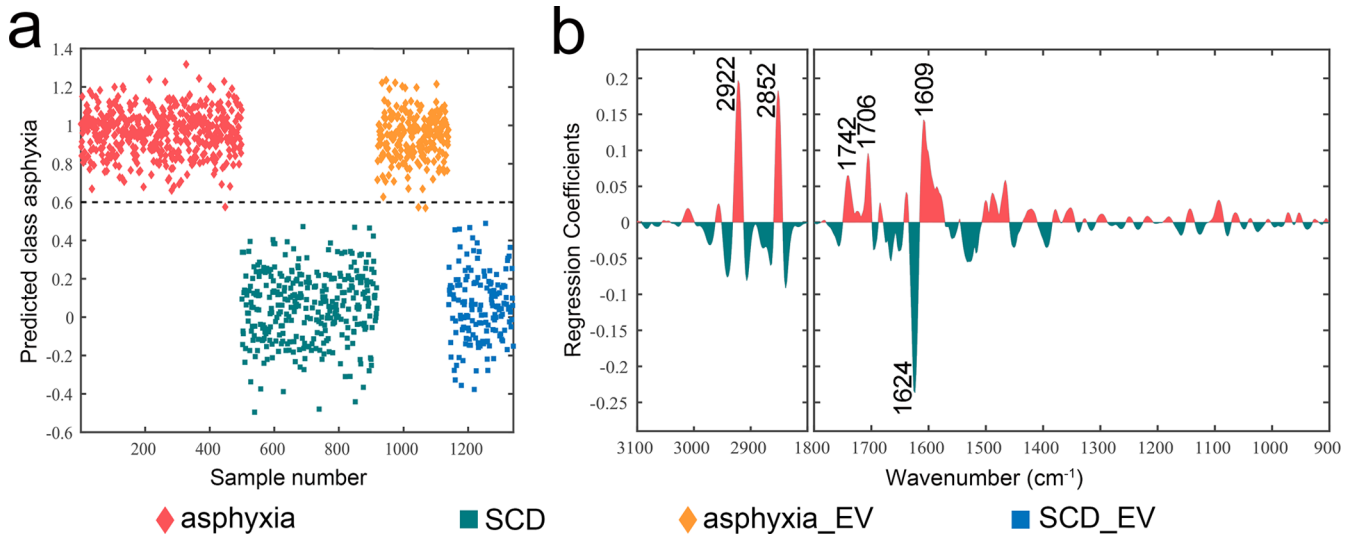

Figure 3. Results of the PLS-DA model built using fresh lung tissues in rats (collected 0 h postmortem). (a) CV and prediction score results. The classification threshold is shown by the black dotted line. (b) Regression coefficients for the PLS-DA model. The "EV" represents the spectra in the external validation/prediction set. SCD: sudden cardiac death.

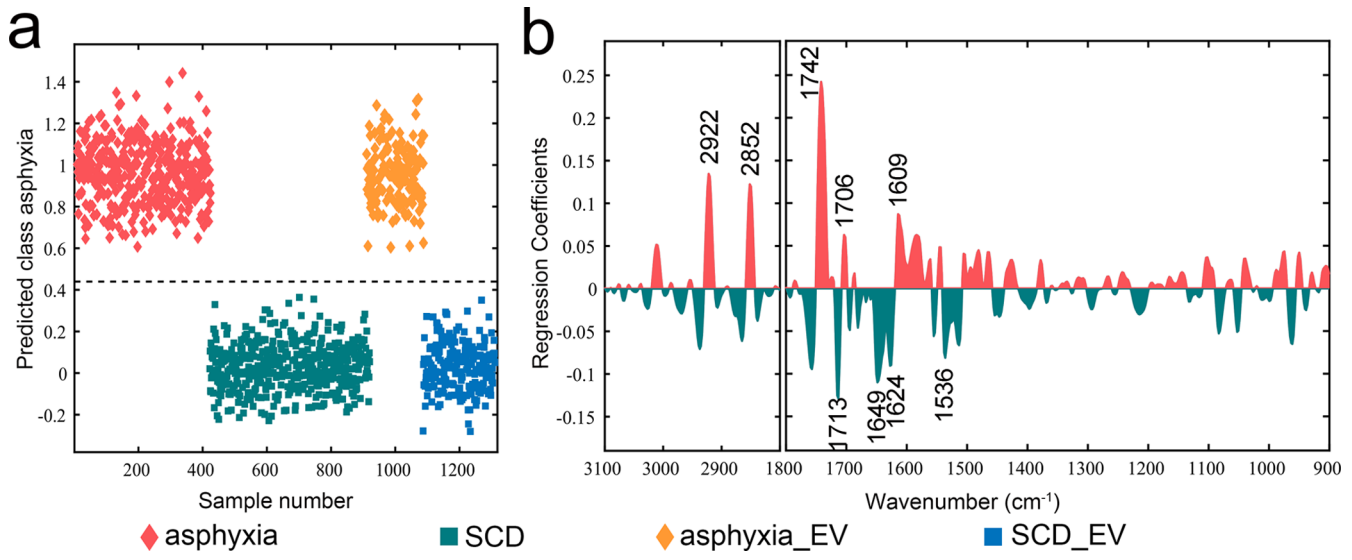

Figure 4. Results of the PLS-DA model built using decomposed lung tissues in rats (collected 24 h postmortem). (a) CV and prediction score results. The classification threshold is shown by the black dotted line. (b) Regression coefficients for the PLS-DA model. The "EV" represents the spectra in the external validation/prediction set. SCD: sudden cardiac death.

also compared. As shown in Figure 6a, we found that seven of the nine bands have the same significant differences as those in the animal dataset, while the band at 1742 cm^{-1} shows the opposite quantitative relationship (the relative intensity of the asphyxia group is greater than that of the SCD group in the animal data but is smaller in the human data), and the band at 1649 cm^{-1} shows no significant differences ($P > 0.05$). The human sample spectral dataset was randomly divided into the calibration and external validation/prediction sets. These seven differential bands were used to build classification models.

At first, we established a PLS-DA model, and the results are shown in Figure S4. The prediction performance was not satisfactory, with an accuracy of 0.653 and an AUC of 0.732. The model gave a sensitivity of 0.845 and a low specificity of 0.490 at the optimal threshold. Next, to improve the prediction performance, a non-linear SVM-DA model was built. In Figure 6b, each point represents a single spectrum, and the probability that it belongs to the asphyxia group is shown by the SVM-DA model. We found that most of the spectrum was correctly classified in both the CV and prediction processes. The confusion matrices of CV and prediction are presented in Figure 6c,d. The model accuracy of prediction was improved to 0.798. The ROC curve and the comparison of AUCs were shown in Figure S5. The AUC of the SVM-DA model was significantly improved to 0.794 ($P = 0.00187$, DeLong's test), which gave a sensitivity of 0.856 and a specificity of 0.748 at the optimal threshold. Statistics on the classification of all spectra in each case are shown in Figure S6.

DISCUSSION

In this study, the spectral profiles of the lung tissues of rats that died from asphyxia and SCD were collected and analyzed to explore the spectral differences and to build a classification

https://doi.org/10.1021/acsomega.2c05968
ACS Omega 2022, 7, 46859−46869

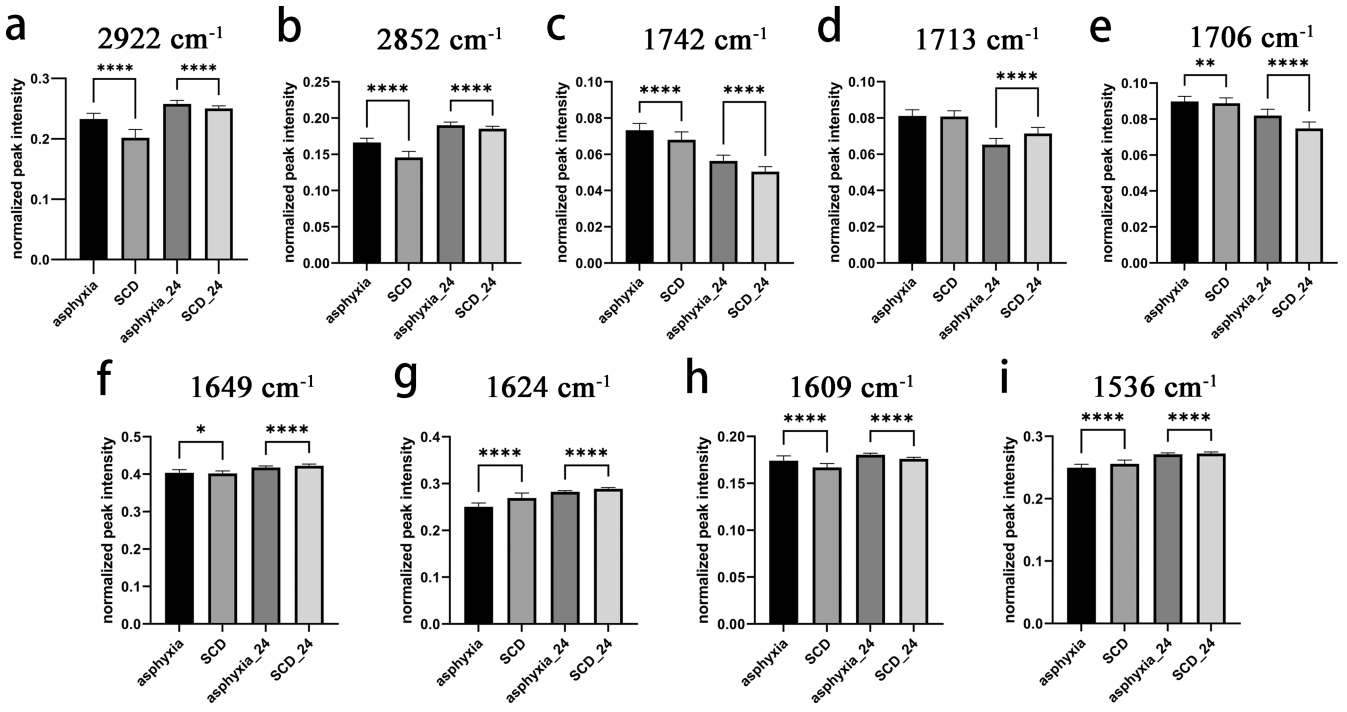

Figure 5. Comparison of the relative peak intensities of nine differential spectral variables in rats between the two causes of death at 0 and 24 h postmortem. ****$P < 0.0001$, **$P < 0.01$, *$P < 0.05$. SCD: sudden cardiac death.

model for the two complex causes of death. The situation when decomposition occurred was also considered.

The averaged original spectra of the two causes of death are very similar, and the second-derivative spectra with less spectral overlapping are also very similar. But a clear distinction trend between the spectra in the two groups was observed by an unsupervised pattern recognition algorithm, which is PCA. This suggests that the biomolecular differences in the lung tissues derived from different causes of death may be subtle, but they do exist and can be detected by the FTIR microspectroscopy technique combined with chemometrics.

Based on the regression coefficients of the PLS-DA model, the biomacromolecule basis of the discrimination can be explored. In the lipid region (3100−2800 cm^{-1}), the most pronounced positive absorption bands at 2922 and 2852 cm^{-1} represent the asymmetric and symmetric stretching vibrations of CH_2 of acyl chains in lipids, respectively.[58] The sum of the peak intensities of CH_2 asymmetric and symmetric stretching vibrations can represent the content of total lipids.[59] In addition, the positive absorption band at 1742 cm^{-1} may originate from the C═O stretching vibration of lipid esters.[60,61] These results may suggest more lipids in the lung cells of rats that died from asphyxia than in those in the SCD group. IuS and Vi found that a high level of lipids in pulmonary tissue from newborns could be evidence of intrauterine asphyxia.[62] Their findings are in accordance with our results.

The absorption bands in the region of 1700−1500 cm^{-1} are dominated by amide I (C═O stretching) and amide II (N−H, C−N stretching) of proteins.[63] A lot of positive and negative absorption bands can be observed in this region. The intensities of absorption bands around 1650 (amide I) and 1550 (amide II) can represent the total protein level, but they are not pronounced in the regression coefficients plot. These results may suggest that the difference in protein composition or protein secondary structure, compared to the difference in protein content, is more obvious in the lung cells between the two causes of death groups. For example, the negatively correlated absorption band at 1624 cm^{-1} is probably assigned to the β-sheet structure of proteins.[64] It may indicate fewer β-sheet-rich proteins in the lung tissues of the asphyxia group than that of the SCD group. The protein aggregation process may lead to more formation of β-sheet structure,[65] so the absorption band around 1624 cm^{-1} can represent the level of aggregated proteins,[66] which could be attributed to tissue ischemia.[67] Therefore, in our results, the difference of 1624 cm^{-1} may result from subtle differences between ischemic and hypoxic processes in different causes of death.

However, it should be emphasized that the nucleic acid bases also contribute to absorption bands in the 1800−1550 cm^{-1} region (due to the C═O, N−H, and C−N stretching modes),[68] though the degree of contribution may be low in the fingerprint region. Due to the complexity of the samples, it is unrealistic to make a definitive assignment in this study. Therefore, the spectral differences can also be attributed to the differences in nucleic acid bases. For example, the positively correlated bands around 1706 and 1609 cm^{-1} may represent the C═O stretching vibrations of thymine and adenine, respectively.[68,69] As mentioned in the Introduction section, some differentially expressed mRNAs and miRNAs have been reported during asphyxia. Therefore, there might be a difference in mRNA or miRNA expression between the death processes of asphyxia and SCD, and it also contributed to the distinction between asphyxia and SCD.

Before exploring the data of decomposed samples, the classification model built with fresh samples was used to try to distinguish the spectra of decomposed lung samples, but the results were not satisfactory, as shown in Figure S7. The PCA score plot of both the fresh and decomposed lung samples is also shown in Figure S8. It can be observed that the spectral differences between the fresh and decomposed samples were

https://doi.org/10.1021/acsomega.2c05968
ACS Omega 2022, 7, 46859−46869

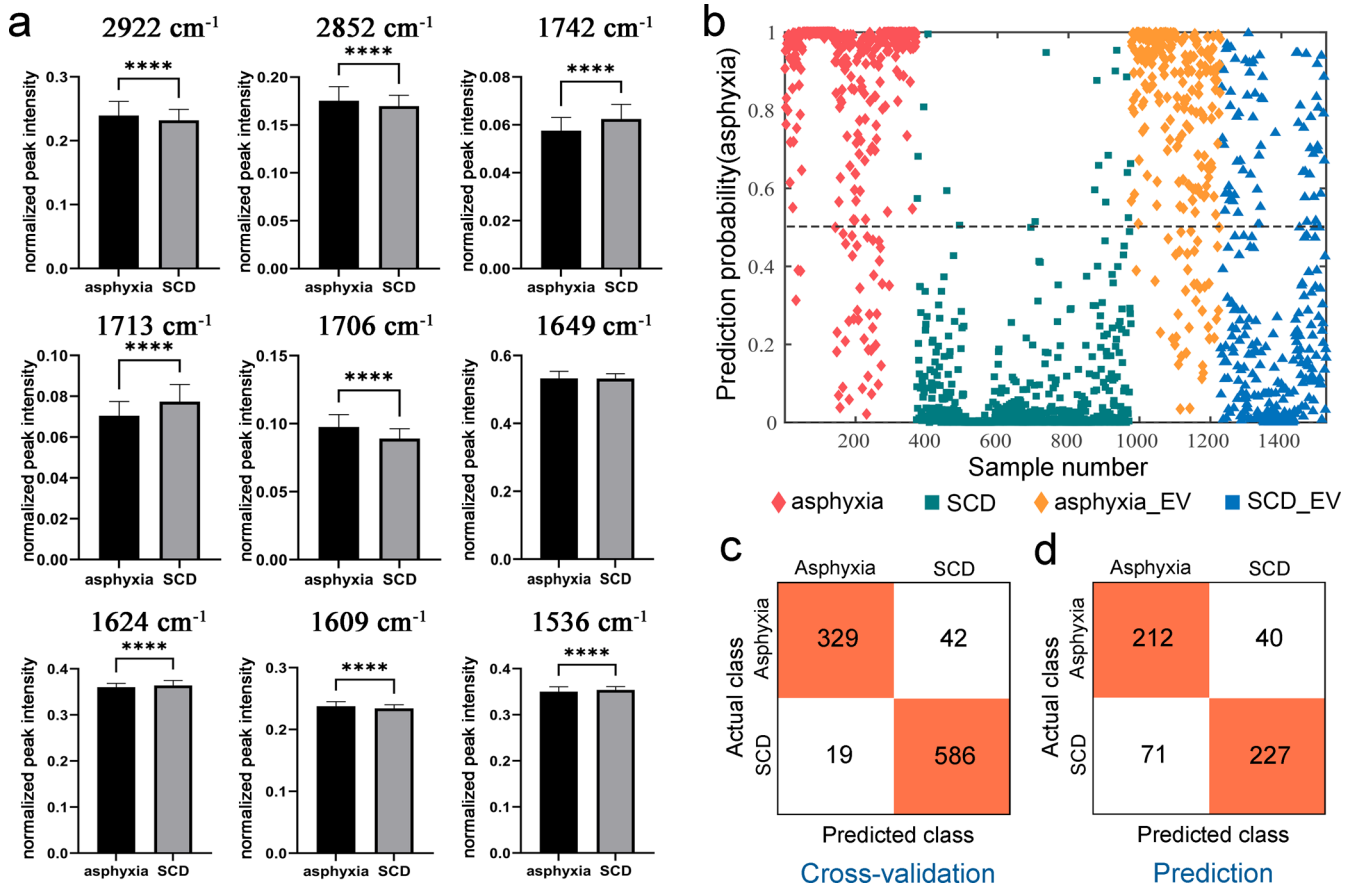

Figure 6. Results of validation in human samples. (a) Comparison between the relative peak intensities of the nine differential spectral variables of the two causes of death in human lung tissues from 16 real cases. ****$P < 0.0001$. (b) CV and external validation/prediction results of the SVM-DA model built using 1526 spectra derived from 16 human lung tissues. The gray dotted line represents the threshold of 50%. The "EV" represents the spectra in the external validation/prediction set. (c) The confusion matrices of CV in the SVM-DA model. (d) The confusion matrices of prediction in the SVM-DA model. SCD: sudden cardiac death.

larger than those between asphyxia and SCD. These results indicate that the decomposition factor may mask the subtle biochemical differences between asphyxia and SCD, affecting their distinction. A previous report from our research group found that the causes of death have no significant effect on predicting PMI using FTIR spectroscopy and chemometrics.[70] In other words, the spectral difference due to the cause of death is much smaller than the spectral difference due to PMI. This point is consistent with the results herein. Therefore, another PLS-DA model was established to explore the discrimination when decomposition occurred by use of the spectra of the asphyxia-decomposed and SCD-decomposed groups.

The spectral differences when decomposition occurred can also be explored based on the regression coefficients of the decomposed PLS-DA model. Several same positively or negatively correlated bands can be observed, although with different regression coefficients, such as the bands at 2922, 2852, 1742, 1706, 1624, and 1609 cm^{-1}. The significant differences in some differential spectral features are maintained even when decomposition has occurred. But the coefficients still differ from the coefficients in the fresh PLS-DA model. The band with the highest coefficient in the fresh PLS-DA model is located at 1624 cm^{-1} (a negatively correlated band), while the highest band in the decomposed PLS-DA model is located at 1742 cm^{-1} (a positively correlated band). This result may indicate that the biomolecular differences that contribute the most to the distinction change from the protein secondary structure to the lipid composition, which might be due to the widespread degradation of proteins and lipids and the microbial behaviors[71−73] (postmortem decomposition includes degradation/autolysis and bacterial putrefaction[74]). Some bands are more pronounced than those in the fresh PLS-DA model, such as 1713, 1649, and 1536 cm^{-1}. The band around 1713 cm^{-1} originates from nucleic acid bases.[68,69] A broad band centered at ∼1650 cm^{-1} is related to amide I of proteins,[63] so the band at 1649 cm^{-1} is probably still due to the difference in protein secondary structure. The band at 1536 cm^{-1} is in the overlapping region of amide II and nucleic acid bases[63,68] and might be attributed to both proteins and nucleic acids. These bands are more pronounced in the regression coefficient plot, possibly because the differences in the macromolecules they represent become larger as the PMI progresses.

Previous research suggests that the height of an absorption band is directly related to the relative content of the corresponding functional groups.[75] Therefore, according to the comparisons of band intensity, we found that (1) the relative contents of some biomolecules increase as decomposition progresses (such as the biomolecules characterized at 2922, 2852, 1649, 1624, 1609, and 1536 cm^{-1}), while some decrease (such as the biomolecules characterized at 1742,

https://doi.org/10.1021/acsomega.2c05968
ACS Omega 2022, 7, 46859−46869

1713, 1706 cm^{-1}); (2) some biomolecules that are significantly different in the fresh samples are still significantly different when decomposition occurs (such as the biomolecules characterized at the eight bands except 1713 cm^{-1}); (3) some biomolecules that are not significantly different in fresh samples but are significantly different in the decomposed samples (such as the biomolecule characterized at 1713 cm^{-1}). Certainly, there must be some biomolecules that are significantly different in fresh samples but are not significantly different in decomposed samples (but this is outside the scope of our study). These results may be due to the degradation of biomolecules, including proteins, lipids, and nucleic acids, and the microbial behaviors mentioned above. Most importantly, there are still significant differences in some spectral features at 24 h postmortem, and a robust classification model can still be established to discriminate asphyxia from SCD based on the differences.

The interpretation of the biomolecular differences represented by spectral features is not the focus of this study. The focus is on how we can screen the differential spectral variables, especially after death, to build a cause-of-death diagnosis model. The calibration and prediction performances of the two PLS-DA models are satisfactory. This indicates that those subtle spectral differences can be utilized to construct classification models to distinguish the lung tissues of rats that died from asphyxia or SCD, even when decomposition has occurred. Although we only investigated the differences and diagnostic abilities of some spectral features at 24 h postmortem in this research, the positive results are inspiring and offer a new perspective for considering the effect of decomposition after death.

And more importantly, we are glad to find that the patterns obtained through systematic and standardized animal experiments were basically validated in human samples in this preliminary study. Seven of the nine bands, except bands at 1742 and 1649 cm^{-1}, exhibit the same significant differences in both the human and animal datasets. A linear PLS-DA model was built in the human dataset at first, but it showed poor performance in both the calibration set and prediction set. This indicates that the PLS-DA model was underfitting. It may be that the variation between human data is larger than that between standardized animals, leading to the fact that the relatively simple linear classifier cannot deal with the complex human sample well. Subsequently, a non-linear SVM-DA model was built, and the AUC value was significantly improved. This model performed well in both the calibration and prediction sets with a prediction accuracy of 0.798. Although that is still not a particularly high number, most of the spectra can be classified correctly. Therefore, if we set the diagnostic criteria as "the class/group that more than 50% of the spectrum is divided into", the cause of death is correctly diagnosed in every case, as shown in Figure S6.

This research has two advantages, which are also limitations. First, in addition to fresh lung tissues, we assessed the biochemical differences in the lung tissues of rats 24 h postmortem. However, the PMI range of corpses may be longer in practice. Therefore, the applicability of this approach to a longer PMI range needs to be further studied. Second, we collected human samples to validate the results of animal experiments, but the study was still limited by the number of human samples. Age, sex, individual differences, and health conditions might be potential factors that could lead to baseline differences in biochemical status.[76,77] Thus, more human samples should be collected so that we may be able to find more trends in the change of some spectral features or to build a more robust cause-of-death diagnosis model in the future. The study offers a new perspective and method for exploring the determination of complex causes of death even when decomposition has occurred and is therefore very meaningful in forensic practice.

CONCLUSIONS

In summary, the spectral differences in the lung tissues of rats that died from asphyxia and SCD were related to alterations in lipids, proteins, and nucleic acids. The subtle biochemical differences can be used to construct a classification model to distinguish asphyxia from SCD. The significant differences in some differential spectral features are maintained after 24 h of decomposition, and we can still build a PLS-DA model to determine the cause of death. Moreover, seven of the nine differential spectral features were proven to be significantly different in the human lung tissues and showed potential for determining asphyxia in real cases. This study showed that FTIR spectroscopy is a promising tool for exploring the subtle biochemical differences resulting from different death processes and determining the cause of death in practice. It should be emphasized, though, that this is an exploratory study and only 16 real cases were tested.

ASSOCIATED CONTENT

Supporting Information

The Supporting Information is available free of charge at https://pubs.acs.org/doi/10.1021/acsomega.2c05968.

Schematic diagram of the frozen section, H&E staining, and FTIR microspectroscopy detection; comparison of average original spectra; plots of the selection of LVs for PLS-DA models; ROC curves for PLS-DA and SVM-DA models and their comparison by Delong's test; statistics on the classification of all spectra in each real case; effect of decomposition by PCA and PLS-DA; approximate PMIs of the 16 real cases; and main points for the determination of asphyxia and SCD (PDF)

AUTHOR INFORMATION

Corresponding Authors

Zhenyuan Wang − *Department of Forensic Pathology, College of Forensic Medicine, Xi'an Jiaotong University, Xi'an 710061, People's Republic of China;* orcid.org/0000-0003-3561-6414; Phone: +86-029-82655472; Email: wzy218@xjtu.edu.cn

Ping Huang − *Shanghai Key Laboratory of Forensic Medicine, Shanghai Forensic Service Platform, Academy of Forensic Science, Shanghai 200063, People's Republic of China;* Phone: +86-021-52367986; Email: huangp@ssfjd.cn

Authors

Kai Zhang − *Department of Forensic Pathology, College of Forensic Medicine, Xi'an Jiaotong University, Xi'an 710061, People's Republic of China*

Ruina Liu − *Department of Forensic Pathology, College of Forensic Medicine, Xi'an Jiaotong University, Xi'an 710061, People's Republic of China*

Ya Tuo − *Department of Biochemistry and Physiology, Shanghai University of Medicine and Health Sciences, Shanghai 201318, People's Republic of China*

https://doi.org/10.1021/acsomega.2c05968
ACS Omega 2022, 7, 46859−46869

Kaijun Ma − *Shanghai Key Laboratory of Crime Scene Evidence, Institute of Criminal Science and Technology, Shanghai Municipal Public Security Bureau, Shanghai 200042, People's Republic of China*

Dongchuan Zhang − *Shanghai Key Laboratory of Crime Scene Evidence, Institute of Criminal Science and Technology, Shanghai Municipal Public Security Bureau, Shanghai 200042, People's Republic of China*

Complete contact information is available at: https://pubs.acs.org/10.1021/acsomega.2c05968

Author Contributions

K.Z. and R.L. contributed equally to this work. K.Z. and P.H. designed the study; K.Z., R.L., and D.Z. performed the measurements and analyzed the data; P.H. and K.M. provided the instruments; K.Z. and Y.T. wrote the manuscript; and Z.W. and P.H. supervised the projects. All authors read and approved the final manuscript.

Funding

This work was supported by the National Natural Science Foundation of China (81730056, 81722027, and 82072115), the National Key R&D Program of China (2022YFC3302002), and the Science and Technology Committee of Shanghai Municipality (21DZ2270800 and 19DZ2292700).

Notes

The authors declare no competing financial interest.

This work was approved by the Laboratory Animal Management Committee of Xi'an Jiaotong University (no. 2017-388) and all procedures were performed in compliance with the recommendations in the Guide for the Care and Use of Laboratory Animals Committee of Xi'an Jiaotong University.

Informed consent was obtained from relatives of the dead about the human samples involved in this study.

Data associated with this manuscript have been archived in the Dryad Digital Repository (https://datadryad.org/stash/share/Cme_r9zFAfaodzhw30bn9r9WYpP5I-76Pc-lVm-uCY0).

REFERENCES

(1) Mosek, D. P.; Sperhake, J. P.; Edler, C.; Püschel, K.; Schröder, A. S. Cases of asphyxia in children and adolescents: a retrospective analysis of fatal accidents, suicides, and homicides from 1998 to 2017 in Hamburg, Germany. *Int. J. Leg. Med.* **2020**, *134*, 1073−1081.

(2) Fracasso, T.; Vennemann, M.; Vennemann, M.; Klöcker, T.; Bajanowski, B.; Brinkmann, H.; Pfeiffer, S. I. D. G. Petechial bleedings in sudden infant death. *Int. J. Leg. Med.* **2011**, *125*, 205−210.

(3) Püschel, K.; Turk, E. E.; Lach, H. Asphyxia-related deaths. *Forensic Sci. Int.* **2004**, *144*, 211−215.

(4) Ma, J.; Jing, H.; Zeng, Y.; Tao, L.; Yang, Y.; Ma, K.; Chen, L. Retrospective analysis of 319 hanging and strangulation cases between 2001 and 2014 in Shanghai. *J. Forensic Leg. Med.* **2016**, *42*, 19−24.

(5) Azmak, D. Asphyxial Deaths: A Retrospective Study and Review of the Literature. *Am. J. Forensic Med. Pathol* **2006**, *27*, 134−144.

(6) Kong, M. H.; Fonarow, G. C.; Peterson, E. D.; Curtis, A. B.; Hernandez, A. F.; Sanders, G. D.; Thomas, K. L.; Hayes, D. L.; Al-Khatib, S. M. Systematic review of the incidence of sudden cardiac death in the United States. *J. Am. Coll. Cardiol.* **2011**, *57*, 794−801.

(7) Feng, X.-F.; Hai, J.-J.; Ma, Y.; Wang, Z.-Q.; Tse, H.-F. Sudden cardiac death in mainland China: a systematic analysis. *Circ.: Arrhythmia Electrophysiol.* **2018**, *11*, No. e006684.

(8) Zeng, Y.; Tao, L.; Ma, J.; Han, L.; Lv, Y.; Hui, P.; Zhang, H.; Ma, K.; Xiao, B.; Shi, Q.; Xu, H.; Chen, L. DUSP1 and KCNJ2 mRNA upregulation can serve as a biomarker of mechanical asphyxia-induced death in cardiac tissue. *Int. J. Leg. Med.* **2018**, *132*, 655−665.

(9) Zeng, Y.; Lv, Y.; Tao, L.; Ma, J.; Zhang, H.; Xu, H.; Xiao, B.; Shi, Q.; Ma, K.; Chen, L. G6PC3, ALDOA and CS induction accompanies mir-122 down-regulation in the mechanical asphyxia and can serve as hypoxia biomarkers. *Oncotarget* **2016**, *7*, 74526−74536.

(10) Han, L.; Zhang, H.; Zeng, Y.; Lv, Y.; Tao, L.; Ma, J.; Xu, H.; Ma, K.; Shi, Q.; Xiao, B.; Chen, L. Identification of the miRNA-3185/CYP4A11 axis in cardiac tissue as a biomarker for mechanical asphyxia. *Forensic Sci. Int.* **2020**, *311*, 110293.

(11) Han, L.; Li, W.; Hu, Y.; Zhang, H.; Ma, J.; Ma, K.; Xiao, B.; Fei, G.; Zeng, Y.; Tian, L.; Chen, L. Model for the prediction of mechanical asphyxia as the cause of death based on four biological indexes in human cardiac tissue. *Sci. Justice* **2021**, *61*, 221−226.

(12) Zhu, B. L.; Ishida, K.; Fujita, M. Q.; Maeda, H. Immunohistochemical investigation of a pulmonary surfactant in fatal mechanical asphyxia. *Int. J. Leg. Med.* **2000**, *113*, 268−271.

(13) Cecchi, R.; Sestili, C.; Prosperini, G.; Cecchetto, G.; Vicini, E.; Viel, G.; Muciaccia, B. Markers of mechanical asphyxia: immunohistochemical study on autoptic lung tissues. *Int. J. Leg. Med.* **2014**, *128*, 117−125.

(14) Zhao, D.; Ishikawa, T.; Quan, L.; Li, D.-R.; Michiue, T.; Yoshida, C.; Komatu, A.; Chen, J.-H.; Zhu, B.-L.; Maeda, H. Tissue-specific differences in mRNA quantification of glucose transporter 1 and vascular endothelial growth factor with special regard to death investigations of fatal injuries. *Forensic Sci. Int.* **2008**, *177*, 176−183.

(15) Wang, Q.; Ishikawa, T.; Michiue, T.; Zhu, B.-L.; Guan, D.-W.; Maeda, H. Intrapulmonary aquaporin-5 expression as a possible biomarker for discriminating smothering and choking from sudden cardiac death: A pilot study. *Forensic Sci. Int.* **2012**, *220*, 154−157.

(16) Zhang, H.; Hu, Y.; Wang, H.; Tian, L.; Li, W.; Han, L.; Xu, H.; Ma, J.; Ma, K.; Xiao, B.; Chen, L. Cytoplasmic upregulation of Cyto c and AIF serve as biomarkers of mechanical asphyxia death. *Am. J. Transl. Res.* **2019**, *11*, 4568−4583.

(17) Gutjahr, E.; Madea, B. Inflammatory reaction patterns of the lung as a response to alveolar hypoxia and their significance for the diagnosis of asphyxiation. *Forensic Sci. Int.* **2019**, *297*, 315−325.

(18) Sabatasso, S.; Mangin, P.; Fracasso, T.; Moretti, M.; Docquier, M.; Djonov, V. Early markers for myocardial ischemia and sudden cardiac death. *Int. J. Leg. Med.* **2016**, *130*, 1265−1280.

(19) Chen, J.-H.; Michiue, T.; Ishikawa, T.; Maeda, H. Pathophysiology of sudden cardiac death as demonstrated by molecular pathology of natriuretic peptides in the myocardium. *Forensic Sci. Int.* **2012**, *223*, 342−348.

(20) Campobasso, C. P.; Dell'Erba, A. S.; Addante, A.; Zotti, F.; Marzullo, A.; Colonna, M. F. Sudden cardiac death and myocardial ischemia indicators: a comparative study of four immunohistochemical markers. *Am. J. Forensic Med. Pathol* **2008**, *29*, 154−161.

(21) Carvajal-Zarrabal, O.; Hayward-Jones, P. M.; Nolasco-Hipolito, C.; Barradas-Dermitz, D. M.; Calderón-Garcidueñas, A. L.; López-Amador, N. Use of cardiac injury markers in the postmortem diagnosis of sudden cardiac death. *J. Forensic Sci.* **2017**, *62*, 1332−1335.

(22) Zhang, K.; Yan, H.; Liu, R.; Xiang, P.; Deng, K.; Zhang, J.; Tuo, Y.; Wang, Z.; Huang, P. Exploring metabolic alterations associated with death from asphyxia and the differentiation of asphyxia from sudden cardiac death by GC-HRMS-based untargeted metabolomics. *J. Chromatogr. B: Anal. Technol. Biomed. Life Sci.* **2021**, *1171*, 122638.

(23) Zhang, K.; Yan, H.; Liu, R.; Xiang, P.; Zhang, J.; Deng, K.; Huang, P.; Wang, Z. The Use of Gas Chromatography Coupled with High-Resolution Mass Spectrometry-Based Untargeted Metabolomics to Discover Metabolic Changes and Help in the Determination of Complex Causes of Death: A Preliminary Study. *ACS Omega* **2021**, *6*, 2100−2109.

(24) Baker, M. J.; Trevisan, J.; Bassan, P.; Bhargava, R.; Butler, H. J.; Dorling, K. M.; Fielden, P. R.; Fogarty, S. W.; Fullwood, N. J.; Heys, K. A.; Hughes, C.; Lasch, P.; Martin-Hirsch, P. L.; Obinaju, B.; Sockalingum, G. D.; Sulé-Suso, J.; Strong, R. J.; Walsh, M. J.; Wood, B. R.; Gardner, P.; Martin, F. L. Using Fourier transform IR spectroscopy to analyze biological materials. *Nat. Protoc.* **2014**, *9*, 1771.

(25) Wrobel, T. P.; Bhargava, R. Infrared Spectroscopic Imaging Advances as an Analytical Technology for Biomedical Sciences. *Anal. Chem.* **2018**, *90*, 1444−1463.
(26) Nallala, J.; Lloyd, G. R.; Shepherd, N.; Stone, N. High-resolution FTIR imaging of colon tissues for elucidation of individual cellular and histopathological features. *Analyst* **2016**, *141*, 630−639.
(27) Petibois, C.; Desbat, B. Clinical application of FTIR imaging: new reasons for hope. *Trends Biotechnol.* **2010**, *28*, 495−500.
(28) Movasaghi, Z.; Rehman, S.; ur Rehman, D. I. Fourier Transform Infrared (FTIR) Spectroscopy of Biological Tissues. *Appl. Spectrosc. Rev.* **2008**, *43*, 134−179.
(29) Gajjar, K.; Heppenstall, L. D.; Pang, W.; Ashton, K. M.; Trevisan, J.; Patel, I. I.; Llabjani, V.; Stringfellow, H. F.; Martin-Hirsch, P. L.; Dawson, T.; Martin, F. L. Diagnostic segregation of human brain tumours using Fourier-transform infrared and/or Raman spectroscopy coupled with discriminant analysis. *Anal. Methods* **2013**, *5*, 89−102.
(30) Verdonck, M.; Denayer, A.; Delvaux, B.; Garaud, S.; De Wind, R.; Desmedt, C.; Sotiriou, C.; Willard-Gallo, K.; Goormaghtigh, E. Characterization of human breast cancer tissues by infrared imaging. *Analyst* **2016**, *141*, 606−619.
(31) Mu, X.; Kon, M.; Ergin, A.; Remiszewski, S.; Akalin, A.; Thompson, C. M.; Diem, M. Statistical analysis of a lung cancer spectral histopathology (SHP) data set. *Analyst* **2015**, *140*, 2449−2464.
(32) Kuepper, C.; Großerueschkamp, F.; Kallenbach-Thieltges, A.; Mosig, A.; Tannapfel, A.; Gerwert, K. Label-free classification of colon cancer grading using infrared spectral histopathology. *Faraday Discuss.* **2016**, *187*, 105−118.
(33) Witzke, K. E.; Großerueschkamp, F.; Jütte, H.; Horn, M.; Roghmann, F.; von Landenberg, N.; Bracht, T.; Kallenbach-Thieltges, A.; Käfferlein, H.; Brüning, T.; Schork, K.; Eisenacher, M.; Marcus, K.; Noldus, J.; Tannapfel, A.; Sitek, B.; Gerwert, K. Integrated Fourier transform infrared imaging and proteomics for identification of a candidate histochemical biomarker in bladder cancer. *Am. J. Pathol.* **2019**, *189*, 619−631.
(34) Muro, C. K.; Doty, K. C.; Bueno, J.; Halámková, L.; Lednev, I. K. Vibrational spectroscopy: recent developments to revolutionize forensic science. *Anal. Chem.* **2015**, *87*, 306−327.
(35) Alkhuder, K. Attenuated total reflection-Fourier transform infrared spectroscopy: a universal analytical technique with promising applications in forensic analyses. *Int. J. Leg. Med.* **2022**, *136*, 1717−1736.
(36) Wang, Q.; Li, W.; Liu, R.; Zhang, K.; Zhang, H.; Fan, S.; Wang, Z. Human and non-human bone identification using FTIR spectroscopy. *Int. J. Leg. Med.* **2019**, *133*, 269−276.
(37) Zhang, K.; Zhang, A.; Liu, R.; Zhang, H.; Lin, H.; Zhang, P.; Huang, P.; Wang, Z. Identifying muscle hemorrhage in rat cadavers with advanced decomposition by FT-IR microspectroscopy combined with chemometrics. *Leg. Med.* **2020**, *47*, 101748.
(38) Lin, H.; Wang, Z.; Luo, Y.; Sun, Q.; Shen, Y.; Huang, P. Postmortem evaluation of the pathological degree of myocardial infarction by Fourier transform infrared microspectroscopy. *Spectrochim. Acta, Part A* **2022**, *268*, 120630.
(39) Yu, K.; Wang, G.; Cai, W.; Wu, D.; Wei, X.; Zhang, K.; Liu, R.; Sun, Q.; Wang, Z. Identification of antemortem, perimortem and postmortem fractures by FTIR spectroscopy based on a rabbit tibial fracture model. *Spectrochim. Acta, Part A* **2020**, *239*, 118535.
(40) Wu, H.; Li, Z.; Liang, X.; Chen, R.; Yu, K.; Wei, X.; Wang, G.; Cai, W.; Li, H.; Sun, Q.; Wang, Z. Pathological and ATR-FTIR spectral changes of delayed splenic rupture and medical significance. *Spectrochim. Acta, Part A* **2022**, *278*, 121286.
(41) Lin, H.; Luo, Y.; Sun, Q.; Zhang, J.; Tuo, Y.; Zhang, Z.; Wang, L.; Deng, K.; Chen, Y.; Huang, P.; Wang, Z. Identification of Pulmonary Edema in Forensic Autopsy Cases of Sudden Cardiac Death Using Fourier Transform Infrared Microspectroscopy: A Pilot Study. *Anal. Chem.* **2018**, *90*, 2708−2715.
(42) Lin, H.; Luo, Y.; Wang, L.; Deng, K.; Sun, Q.; Fang, R.; Wei, X.; Zha, S.; Wang, Z.; Huang, P. Identification of pulmonary edema in forensic autopsy cases of fatal anaphylactic shock using Fourier transform infrared microspectroscopy. *Int. J. Leg. Med.* **2018**, *132*, 477−486.
(43) Lin, H.; Guo, X.; Luo, Y.; Chen, Y.; Zhao, R.; Guan, D.; Wang, Z.; Huang, P. Postmortem Diagnosis of Fatal Hypothermia by Fourier Transform Infrared Spectroscopic Analysis of Edema Fluid in Formalin-Fixed, Paraffin-Embedded Lung Tissues. *J. Forensic Sci.* **2020**, *65*, 846−854.
(44) Wu, D.; Luo, Y.-W.; Zhang, J.; Luo, B.; Zhang, K.; Yu, K.; Liu, R.-N.; Lin, H.-C.; Wei, X.; Wang, Z.-Y.; Huang, P. Fourier-transform infrared microspectroscopy of pulmonary edema fluid for postmortem diagnosis of diabetic ketoacidosis. *Spectrochim. Acta, Part A* **2021**, *258*, 119882.
(45) Tuo, Y.; Zhang, K.; Wang, L.; Luo, Y.; Sun, Q.; Lin, H.; Zhang, Z.; Chen, Y.; Sun, J.; Huang, P. Characterization and postmortem diagnosis of fatal heatstroke using Attenuated Total Reflectance Fourier transform infrared spectroscopy combined with chemometrics. *Spectrosc. Lett.* **2020**, *53*, 372−382.
(46) Wang, Z.; Tuo, Y.; Li, B.; Deng, K.; Han, S.; Luo, Y.; Sun, Q.; Li, Z.; Chen, Y.; Wang, Z.; Huang, P. Preliminary study on fatal hyperthermia in rat liver tissue by Fourier transform infrared microspectroscopy. *Aust. J. Forensic Sci.* **2017**, *49*, 468−478.
(47) Zhou, C.; Byard, R. W. Factors and processes causing accelerated decomposition in human cadavers − An overview. *J. Forensic Leg. Med.* **2011**, *18*, 6−9.
(48) Lasch, P. Spectral pre-processing for biomedical vibrational spectroscopy and microspectroscopic imaging. *Chemom. Intell. Lab. Syst.* **2012**, *117*, 100−114.
(49) Trevisan, J.; Angelov, P. P.; Carmichael, P. L.; Scott, A. D.; Martin, F. L. Extracting biological information with computational analysis of Fourier-transform infrared (FTIR) biospectroscopy datasets: current practices to future perspectives. *Analyst* **2012**, *137*, 3202−3215.
(50) Martens, H.; Stark, E. Extended multiplicative signal correction and spectral interference subtraction: new preprocessing methods for near infrared spectroscopy. *J. Pharm. Biomed. Anal.* **1991**, *9*, 625−635.
(51) Martin, F. L.; Kelly, J. G.; Llabjani, V.; Martin-Hirsch, P. L.; Patel, I. I.; Trevisan, J.; Fullwood, N. J.; Walsh, M. J. Distinguishing cell types or populations based on the computational analysis of their infrared spectra. *Nat. Protoc.* **2010**, *5*, 1748−1760.
(52) Bro, R.; Smilde, A. K. Principal component analysis. *Anal. Methods* **2014**, *6*, 2812−2831.
(53) Næs, T.; Isaksson, T.; Fearn, T.; Davies, T. *A User-Friendly Guide to Multivariate Calibration and Classification*; NIR: Chichester, 2002; Vol. *6*.
(54) Ballabio, D.; Consonni, V. Classification tools in chemistry. Part 1: linear models. PLS-DA. *Anal. Methods* **2013**, *5*, 3790−3798.
(55) Westerhuis, J. A.; Hoefsloot, H. C. J.; Smit, S.; Vis, D. J.; Smilde, A. K.; van Velzen, E. J. J.; van Duijnhoven, J. P. M.; van Dorsten, F. A. Assessment of PLSDA cross validation. *Metabolomics* **2008**, *4*, 81−89.
(56) DeLong, E. R.; DeLong, D. M.; Clarke-Pearson, D. L. Comparing the areas under two or more correlated receiver operating characteristic curves: a nonparametric approach. *Biometrics* **1988**, *44*, 837−845.
(57) Sun, X.; Xu, W. Fast Implementation of DeLong's Algorithm for Comparing the Areas Under Correlated Receiver Operating Characteristic Curves. *IEEE Signal Process. Lett.* **2014**, *21*, 1389−1393.
(58) Caine, S.; Heraud, P.; Tobin, M. J.; McNaughton, D.; Bernard, C. C. A. The application of Fourier transform infrared microspectroscopy for the study of diseased central nervous system tissue. *Neuroimage* **2012**, *59*, 3624−3640.
(59) Cakmak, G.; Miller, L. M.; Zorlu, F.; Severcan, F. Amifostine, a radioprotectant agent, protects rat brain tissue lipids against ionizing radiation induced damage: An FTIR microspectroscopic imaging study. *Arch. Biochem. Biophys.* **2012**, *520*, 67−73.
(60) Sukuta, S.; Bruch, R. Factor analysis of cancer Fourier transform infrared evanescent wave fiberoptical (FTIR-FEW) spectra. *Laser Surg. Med.* **1999**, *24*, 382−388.

https://doi.org/10.1021/acsomega.2c05968
ACS Omega 2022, 7, 46859−46869

(61) Yoshida, S.; Miyazaki, M.; Sakai, K.; Takeshita, M.; Yuasa, S.; Sato, A.; Kobayashi, T.; Watanabe, S.; Okuyama, H. Fourier transform infrared spectroscopic analysis of rat brain microsomal membranes modified by dietary fatty acids: Possible correlation with altered learning behavior. *Biospectroscopy* **1997**, *3*, 281−290.
(62) IuS, P.; Vi, A. The diagnosis of intrauterine asphyxia by the lipid content in the lungs of the cadavers of newborn infants using fresh and putrefied material. *Sud.-Med. Ekspert.* **1994**, *37*, 12.
(63) Baker, M. J.; Hussain, S. R.; Lovergne, L.; Untereiner, V.; Hughes, C.; Lukaszewski, R. A.; Thiéfin, G.; Sockalingum, G. D. Developing and understanding biofluid vibrational spectroscopy: a critical review. *Chem. Soc. Rev.* **2016**, *45*, 1803−1818.
(64) Kong, J.; Yu, S. Fourier Transform Infrared Spectroscopic Analysis of Protein Secondary Structures. *Acta Biochim. Biophys. Sin.* **2007**, *39*, 549−559.
(65) Shivu, B.; Seshadri, S.; Li, J.; Oberg, K. A.; Uversky, V. N.; Fink, A. L. Distinct β-Sheet Structure in Protein Aggregates Determined by ATR−FTIR Spectroscopy. *Biochemistry* **2013**, *52*, 5176−5183.
(66) Hackett, M. J.; DeSouza, M.; Caine, S.; Bewer, B.; Nichol, H.; Paterson, P. G.; Colbourne, F. A New Method To Image Heme-Fe, Total Fe, and Aggregated Protein Levels after Intracerebral Hemorrhage. *ACS Chem. Neurosci.* **2015**, *6*, 761−770.
(67) Hackett, M. J.; Britz, C. J.; Paterson, P. G.; Nichol, H.; Pickering, I. J.; George, G. N. In Situ Biospectroscopic Investigation of Rapid Ischemic and Postmortem Induced Biochemical Alterations in the Rat Brain. *ACS Chem. Neurosci.* **2015**, *6*, 226−238.
(68) Dovbeshko, G. I.; Gridina, N. Y.; Kruglova, E. B.; Pashchuk, O. P. FTIR spectroscopy studies of nucleic acid damage. *Talanta* **2000**, *53*, 233−246.
(69) Dovbeshko, G. I.; Chegel, V. I.; Gridina, N. Y.; Repnytska, O. P.; Shirshov, Y. M.; Tryndiak, V. P.; Todor, I. M.; Solyanik, G. I. Surface enhanced IR absorption of nucleic acids from tumor cells: FTIR reflectance study. *Biopolymers* **2002**, *67*, 470−486.
(70) Zhang, K.; Wang, Q.; Liu, R.; Wei, X.; Li, Z.; Fan, S.; Wang, Z. Evaluating the effects of causes of death on postmortem interval estimation by ATR-FTIR spectroscopy. *Int. J. Leg. Med.* **2020**, *134*, 565−574.
(71) Pittner, S.; Monticelli, F. C.; Pfisterer, A.; Zissler, A.; Sänger, A. M.; Stoiber, W.; Steinbacher, P. Postmortem degradation of skeletal muscle proteins: a novel approach to determine the time since death. *Int. J. Leg. Med.* **2016**, *130*, 421−431.
(72) Ueland, M.; Collins, S.; Maestrini, L.; Forbes, S. L.; Luong, S. Fresh vs. frozen human decomposition − A preliminary investigation of lipid degradation products as biomarkers of post-mortem interval. *Forensic Chem.* **2021**, *24*, 100335.
(73) Metcalf, J. L.; Xu, Z. Z.; Weiss, S.; Lax, S.; Van Treuren, W.; Hyde, E. R.; Song, S. J.; Amir, A.; Larsen, P.; Sangwan, N.; Haarmann, D.; Humphrey, G. C.; Ackermann, G.; Thompson, L. R.; Lauber, C.; Bibat, A.; Nicholas, C.; Gebert, M. J.; Petrosino, J. F.; Reed, S. C.; Gilbert, J. A.; Lynne, A. M.; Bucheli, S. R.; Carter, D. O.; Knight, R. Microbial community assembly and metabolic function during mammalian corpse decomposition. *Science* **2016**, *351*, 158−162.
(74) Dowell-Curby, J. *A Review of the Microbiome Associated with Human Decomposition*; Murdoch University, 2017.
(75) Meade, A. D.; Lyng, F. M.; Knief, P.; Byrne, H. J. Growth substrate induced functional changes elucidated by FTIR and Raman spectroscopy in in−vitro cultured human keratinocytes. *Anal. Bioanal. Chem.* **2007**, *387*, 1717−1728.
(76) Murphy, C. Effects of Age and Biochemical Status on Preference for Amino Acids1,b. *Ann. N. Y. Acad. Sci.* **1987**, *510*, 515−518.
(77) Costongs, G. M.; Janson, P. C. W.; Bas, B. M.; Hermans, J.; van Wersch, J. W. J.; Brombacher, P. J. Short-term and long-term intra-individual variations and critical differences of clinical chemical laboratory parameters. *J. Clin. Chem. Clin. Biochem.* **1985**, *23*, 7−16.

https://doi.org/10.1021/acsomega.2c05968
ACS Omega 2022, 7, 46859−46869